IEEE Access
Multidisciplinary | Rapid Review | Open Access Journal

Received January 10, 2021, accepted February 7, 2021, date of publication February 23, 2021, date of current version June 30, 2021.

Digital Object Identifier 10.1109/ACCESS.2021.3061446

Real-Time Array Shape Estimation Method of Horizontal Suspended Linear Array Based on Non-Acoustic Auxiliary Sensors

ZONGLUN CHE, JUN WANG, JING ZHU, BINGBING ZHANG, YANG ZHANG, AND YANQUN WU

College of Meteorology and Oceanography, National University of Defense Technology, Changsha 410073, China

Corresponding author: Jun Wang (wangjunryan@foxmail.com)

This work was support by the Research Program Project of the National University of Defense Technology under Grant ZK19-36.

ABSTRACT The horizontal floating linear array is a new type of array used to detect deep-sea targets. Reliable target detection depends on the estimation accuracy of the array shape. So far, it has been proved that the theoretical array line of the array form is parabolic under ideal conditions. This paper constructs a segmented array estimation method based on the measurement data of the attitude depth sensor. The key of this method is to use the translation invariance of the array curve to establish and solve the underdetermined equation of the segment curve on the array state function. The array curve is segmented according to the sensor and the estimated array curve is obtained by iterative splicing. The simulation data of the horizontal floating array shows that the estimation error of this method is small, and the error optimization analysis of the parameters is carried out in this paper. In addition, this method has good universal applicability so that it can be applied to the formation estimation of other types of arrays.

INDEX TERMS Array shape estimation, horizontal suspension array, translation invariance, non-acoustic auxiliary sensors.

I. INTRODUCTION

At present, traditional hydrophone array forms mainly include side arrays [1], [2], towed arrays [3]–[7], shore-based arrays [8], and vertical arrays [9]. Side arrays and towed arrays are ship-based sonar equipment. They have good maneuverability but are easily affected by ship noise. Shore-based arrays rely on shore station systems and can build large-scale arrays. However, their application situation is fixed, and their application scenario is limited. The vertical array is a form of submarine buoy, and it can be flexibly deployed to realize target autonomous detection. However, the array's scale is generally small, and the deep-sea application technology has not yet achieved a breakthrough. The horizontal suspension hydrophone line array [10] refers to a new type of array in which the linear array of hydrophones is horizontally suspended under water. it combines the advantages of the above-mentioned traditional array. It cannot only realize mobile deployment and autonomous detection but also build large-scale arrays. In addition, it cannot be affected by ship noise and can provide novel means for underwater target detection, especially for submarine detection. Generally, buoy hanging type, ship-mounted hanging type, and rivet hanging type arrays can be used to realize the suspension function [11]. The buoy hanging type is mainly suitable for areas shallower than sea level, and it has certain limitations concerning the array depth. The ship-mounted hanging type is not suitable for horizontal suspension arrays and is more suitable for the suspension of vertical arrays. The rivet hanging type not only can change the suspension depth by changing the rivet rope length, but it can also realize horizontal suspension under ideal conditions through hanging at both ends. Therefore, the rivet suspended horizontal suspension array is more suitable for the study of this paper.

The rivet suspended horizontal suspension array refers to the sonar equipment that allows linear arrays to be sus-pended in seawater through certain constraints to detect underwater targets. The two ends of a linear array are respectively towed using floats and heavy anchors to straighten the array in order to realize horizontal suspension. The schematic diagram is shown in Fig. 1. The depth and attitude sensors (DAS) is the accessory drive system, and it is the main carrier for attitude

The associate editor coordinating the review of this manuscript and approving it for publication was Mohammad Zia Ur Rahman.

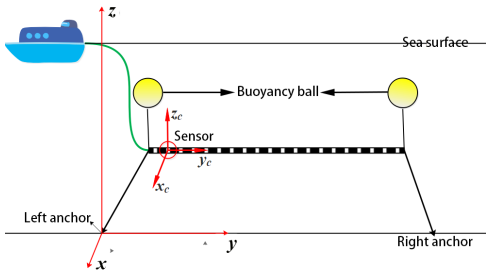

FIGURE 1. Schematic diagram of reference system and carrier coordinate system.

and depth sensors. Using this horizontal line array suspended at a depth of several hundred meters, the effective detection of underwater targets, such as submarines of the same depth, can be realized at a close range.

Methods of array shape estimation mainly include the acoustic calculation method [12]–[19] and the non-acoustic auxiliary measurement method [11], [14], [20]–[29]. The acoustic calculation method uses the underwater acoustic signals received by hydrophone arrays, where it uses the sound source to receive the signals and then deduct the line shape of the array. The non-acoustic auxiliary measurement method entails installing several auxiliary sensors on a line array, such as heading sensors, pressure sensors, etc., and it also uses the sensors to measure the attitude information and depth information of the array to obtain a set of coordinate data of different discrete points on the array. The effective curve fitting method uses numerical simulations to estimate the line type of the array. This type is suitable for arrays with real-time changes in the formation, and the estimation accuracy is limited by the measurement accuracy, the quantity of the sensors, and the accuracy of the formation estimation algorithm.

In the non-acoustic auxiliary measurement method, the interpolation fitting method has the advantages of less calculations, simple system structure, and higher calculation accuracy. By binding multiple auxiliary sensors on a line array, the speed and position status of multiple points on the array can be measured, the measured discrete data can be used to estimate the parameters of the theoretical line type of the assumed array in advance, and then the estimated array curve equation can be obtained. This method is called interpolation fitting. In 1992, B. E. Howard and J. M. Syck proposed the interpolation fitting method using auxiliary sensors for multiple sampling analyses, and they also analyzed the interpolation fitting accuracy in detail [27]. In 2004, Hee-Young Park proposed a new interpolation fitting method to estimate the formation [24]. This method iteratively analyzes and processes the measurement data of auxiliary measurement sensors. Then, it uses a computer model to interpolate the formation information after the analysis and processing. Fitting achieves the purpose of formation estimation. This method greatly improves the accuracy of interpolation fitting to estimate the formation.

It has been solved the array form of the horizontal suspension linear array theoretically using the mechanical equilibrium condition equation through the force analysis of the horizontal suspension linear array structure [10]. This study is based on the conclusion that the formation is parabolic in the zero buoyancy state as a theoretical basis, and the actual array morphological equation is fitted by interpolation through the measurement data of the sensor.

In this paper, the underdetermined equations regarding the formation state function were converted into exactly determined equations by translating the segmented curve, and the final estimated formation curve was obtained using iterative splicing. The biggest advantage of this paper is that the method is relatively simple, suitable for most types of array curve estimations, and has a certain universality.

II. MATHEMATICAL MODEL

Accurate array shape estimation is obtained using actual formation measurements. The method of the accurate estimation of the array shape based on DAS systems refers to one of the most common array shape estimation methods.

A. SYSTEM SETUP AND STATE EQUATIONS

Fig. 1 shows a typical array arrangement of the horizontal floating line array. The coordinate system is established in the figure. The origin of the coordinate system is the anchor point at the left end, and the y-axis is at the initial time (parallel to the initial array line) along the direction of the array, the z-axis is perpendicular to sea level and to the points in the sea level direction. The x-axis and the other two coordinate axes form a right-handed spiral relationship. In the array distortion, it is assumed that the sea surface fluctuation can be ignored, and the sea surface can be regarded as a strict plane. Therefore, in this process, this coordinate system is a fixed coordinate system and cannot change with any sea level changes. The figure also shows the carrier coordinate system with the long axis of the sensor as a coordinate axis, where the y_c-axis follows the long axis of the sensor, and the positive direction is on the array extension direction side. The z_c-axis points toward the upper surface of the sensor and is perpendicular to it. The x_c-axis complies with the short side of the sensor, and the positive directions of the other two axes form a right-handed spiral relationship. The carrier coordinate system is linked to the sensor and moves along with it.

As suggested from the dynamic analysis results of the suspension array, when the suspension array is subjected to the external force of the ocean, its formation is parabolic or catenary. For simplicity, the linear type of the suspension array is assumed to be parabolic, and the projections of this curve on the $x-O-y$ and $z-O-y$ planes are both parabolic.

In Fig. 2, the total number of N attitude and depth sensors are arranged equidistantly in an array of length L.The coordinate of the $k-th$ attitude sensor is assumed as (x_k, y_k, z_k), then the plane curve between any $k-th$ attitude sensor and

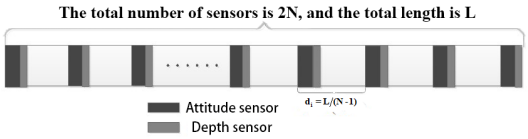

FIGURE 2. A schematic view of the sensor attitude angle defined.

$(k+1)-th$ attitude sensor is a parabola as well, where $k = 1, 2, 3, \ldots, N-1$.

For the $k-th$ curve, $x-O-y$ and the curve on the plane can be expressed as

$$\begin{cases} x_k = a_{x,k}y^2 + b_{x,k}y + c_{x,k} \\ z_k = a_{z,k}y^2 + b_{z,k}y + c_{z,k} \end{cases} \tag{1}$$

where X_k and Z_k represent the projection curve function of the $x-O-y$ plane and $z-O-y$ plane respectively.M_k is the coefficient matrix of the undetermined coefficient equation, and its form is given by Equation.(2). The different elements of Y represent different powers of the independent variable y, as defined in Equation.(3)

$$M_k = \begin{bmatrix} a_{x,k} & b_{x,k} & c_{x,k} \\ a_{z,k} & b_{z,k} & c_{z,k} \end{bmatrix} \tag{2}$$

$$\overline{Y} = \begin{bmatrix} y^2 & y & 1 \end{bmatrix}^T \tag{3}$$

B. RELATIONSHIP BETWEEN ARRAY PARAMETERS AND DAS PARAMETERS

Overall, the attitude sensor is composed of a heading sensor and a 3D motion attitude sensor, which is commonly known as an electronic compass. The required parameters by the attitude sensor consist of the heading yaw angle, pitch angle, and roll angle of the carrier. In the plane parallel to the ground plane through the sensor, the long axis of the sensor initially points toward the 2D angle of the heading direction as the deviation of the array. The pitch of the array is rotated around the short axis of the sensor. Moreover, the roll of the array is rotated around the long axis of the sensor.

As shown in Fig. 3,the three attitude angles of the sensor are defined below:

Yaw angle φ: The angle between the projection line in the horizontal plane of the array extension direction and the true north direction. East by north is positive, and west by north is negative. Its size range is $-180°$ to $180°$.

Pitch angle θ: The angle at which the array rotates around the short axis of the attitude sensor, counterclockwise rotation is positive, and clockwise rotation is negative, and its size ranges from $-90°$ to $90°$.

Roll angle γ: the angle that the array rotates around the long axis of the attitude sensor, counterclockwise is positive, clockwise is negative, and its size ranges from $-180°$ to $180°$.

The depth sensor is capable of exploiting a pressure sensor at this point can be determined by Equation.(4).

$$h = \frac{P - P_0}{\rho g} \tag{4}$$

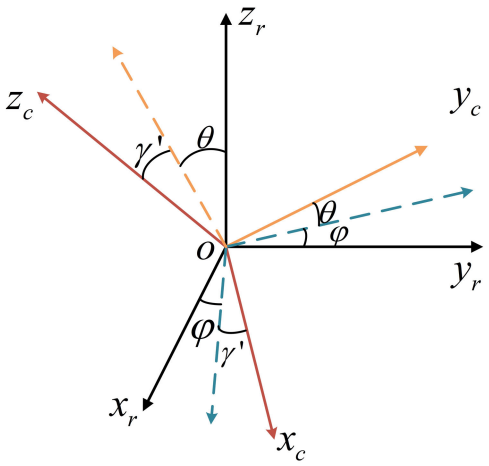

FIGURE 3. A schematic view of the sensor attitude angle defined.

where ρ denotes the density of sea water, P_0 is the atmospheric pressure, g represents the acceleration of gravity at that point.

Suppose that the coordinate of the left end of the array at a certain time is (x_0, y_0, z_0), and the coordinate of the right end is (x_N, y_N, z_N). Considering the $i-th$ sensor, the attitude and depth information acquired through the measurement data of the attitude and depth sensor is $(\theta_i, \gamma_i, \varphi_i, h_i)$. Then the position coordinates of the left end of the $i-th$ sensor element is (x_i, y_i, z_i), The position coordinates at the right end is $(x_i + dx_i, y_i + dy_i, z_i + dz_i)$ as shown in the left of Fig. 4, which (dx_i, dy_i, dz_i) can represent the tangent information of the office at the point of (x_i, y_i, z_i). The relationship between the schematic diagram and the attitude angle is presented in the right of Fig. 4.

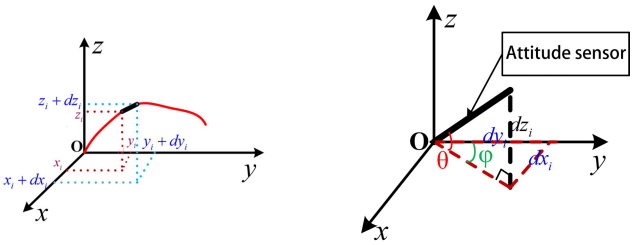

FIGURE 4. Schematic diagram of posture information.

For the cylindrical flexible hydrophone array, the roll angle does not impact the shape of the array curve. Thus, only the relationship between the pitch angle, yaw angle, and position coordinate information requires investigation. Complying with the definition of the attitude angle, the pitch angle refers to the angle between the line at which the long axis of the sensor is located and the reference horizontal plane. Also, the deflection angle refers to the angle between the projection line of the line at which the long axis of the sensor is located on the reference horizontal plane and the true north direction. Fig. 4 indicates that the long axis of the attitude

sensor is projected on the horizontal plane. Given the geometric relationship, the measured relationship between the position coordinates of the sensor and the attitude angle is represented by Equation.(5):

$$\begin{cases} \tan\theta_i = \dfrac{dz_i}{\sqrt{dx_i^2 + dy_i^2}} \\ \tan\varphi_i = \dfrac{dx_i}{dy_i} \end{cases} \tag{5}$$

In addition, a relationship is identified between the ordinate of the carrier coordinate system and the depth information.

$$z_i + h_i = H \tag{6}$$

C. SOLUTION OF ARRAY STATE EQUATIONS

Array shape estimation aims to determine the parameter matrix M_k, the coefficients are determined, and the corresponding formation is determined accordingly. To determine the parameters of the coefficient matrix, the coordinates of discrete points on the formation curve or curve tangent information should be known as well. The relationship between the measurement data of the attitude sensor and the tangential information of the formation curve can be determined by Equation.(3).

$$\begin{bmatrix} \mu_k \\ \sigma_k \end{bmatrix} = \begin{bmatrix} \frac{dz_k/dy}{\sqrt{1+(dx_k/dy)^2}} & \frac{dx_k}{dy} \end{bmatrix}^T \tag{7}$$

where μ_k and σ_k respectively represent the end-point tangent slope of the segmented curve of two plane projections. They satisfy $\begin{bmatrix} \mu_k & \sigma_k \end{bmatrix}^T = \begin{bmatrix} \tan\theta_k & \tan\varphi_k \end{bmatrix}^T$.

The relationship between the measurement data of the depth sensor and the coordinate of the curve of the array shape can be obtained from Equation.(7).

$$\begin{bmatrix} x_k \\ z_k \end{bmatrix} = M_k \overline{Y}_k \tag{8}$$

where $\overline{Y}_k$ represents the y-axis coordinate of the end point of the segmented curve.

Moreover, at the junction of two adjacent sub-curves, the formation curve is smooth and continuous, i.e., the coordinates of the two curves at the junction are the same, and the derivative at this point is the same as well. The first type of boundary conditions are written in Equation.(9)

$$M_k \overline{Y}_k = M_{k+1} \overline{Y}_{k+1} \tag{9}$$

and the second type of boundary conditions are written in Equation.(10)

$$\begin{cases} \left.\dfrac{dx_k}{dy}\right|_{y=y_k} = \left.\dfrac{dx_{k+1}}{dy}\right|_{y=y_k} \\ \left.\dfrac{dz_k}{dy}\right|_{y=y_k} = \left.\dfrac{dz_{k+1}}{dy}\right|_{y=y_k} \end{cases} \tag{10}$$

Since the coordinates of one end of the array will exert no effect the curve equation of the array, it can be considered that the coordinates (x_1, y_1, z_1) of the left end of the array are known.

Moreover, for the entire array curve, the total length of the array curve is L. Subsequently,

$$L = \int_{y_1}^{y_N} \sqrt{1 + \left(x_k'\right)^2 + \left(z_k'\right)^2} dy \tag{11}$$

The solution of the above equation can be regarded as a problem of parameter estimation. knowing the coordinates of discrete points, assuming that the curve is a parabola, and using the coordinates of these coordinate points to estimate the parameters of the linear equation. An analytic formation curve is difficult to obtain based on the mentioned equations. It is required to solve the Equations of (7)(8)(9) (10)and (11) which is necessary to use numerical solutions.

As shown in Fig 2, the position coordinates of each attitude sensor before the array is deformed are $(0, L_r \sin\theta_1 + (k-1)L/(N-1), L_r \cos\theta_1)$.The present study mainly studies that the original y axis coordinate of the position of the attitude sensor can be adopted to approximate the y axis coordinate of the distorted sensor position when the array distortion is small.

According to Fig 2, N attitude sensors and depth sensors are installed equidistantly on the array in this model, and the curve equation of the array can be estimated via the following calculation of parameter estimation

The y coordinate of the left end point is known. The data measured with the depth sensor can calculate the z coordinate at this point. Under the constraints of the horizontal floating array, a relational expression is yielded at the left end point:

$$x_1^2 + y_1^2 + z_1^2 = {L_r}^2 \tag{12}$$

Accordingly, the complete coordinates of the left end point can be yielded.

On each sub-curve, the tangent information of the curve at the two ends of the sub-curve can be acquired according to Equation.(13).

Based on the mentioned known conditions, five sets of equations can be listed, just to solve the six unknown parameters in the parameter matrix and subsequently solve the first section of the curve equation. However, the unknowns of each curve segment are greater than the number of equations.

$$\begin{cases} x_j = A_{x,j} \overline{Y}_j \\ z_j = A_{z,j} \overline{Y}_j \\ \mu_j = z_j' \Big/ \sqrt{1 + \left(x_j'\right)^2} \\ \sigma_j = x_j' \end{cases} \tag{13}$$

where j denotes the number of end points of the curve, $A_{x,j}$ and $A_{z,j}$ represent the coefficients of each order of the state function of x_j and z_j respectively. Here $1 \le j \le N-1$, representing the end points of the section of the sub-curve.

$$\begin{cases} A_{x,j} = [\, a_{x,j} \;\; b_{x,j} \;\; c_{x,j} \,] \\ A_{z,j} = [\, a_{z,j} \;\; b_{z,j} \;\; c_{z,j} \,] \end{cases} \tag{14}$$

Since the unknowns of the above equations are the parameters of the coefficient matrix M, there are 6 unknown parameters for each section of the curve, and there are only 5 effective equations. This equation set is an underdetermined equation set, and the solution of the equation set cannot be solved accurately. At the same time, it is also noticed that the curve has the characteristics of translation invariance, that is, the translation of the curve in the coordinate system will not change the shape of the curve, so the left end of each curve segment can be translated to the origin of the coordinate, and then a y-axis will be added. Coordinate equations. At this time, for each segment of the curve, the number of equations is equal to the number of unknowns, and the underdetermined equation group becomes a precisely determined equation group, and the coefficients of each curve segment can be solved.

Solving Equation.(13) can express that the unknown parameters in the parameter matrix are represented by known data, as expressed in Equation.(15).

$$\begin{cases} a_{z,k} = (\kappa_k - \kappa_{k+1})/2\,(y_k - y_{k+1}) \\ b_{z,k} = \kappa_k - (\kappa_k - \kappa_{k+1})/(y_k - y_{k+1}) \\ c_{z,k} = z_k + \left[\kappa_k\left(y_k^2 + 2\right) + \kappa_{k+1}\Delta_k\right]/(y_k - y_{k+1}) \\ a_{x,k} = (\sigma_k - \sigma_{k+1})/2\,(y_k - y_{k+1}) \\ b_{x,k} = \sigma_k - (\sigma_k - \sigma_{k+1})/(y_k - y_{k+1}) \\ c_{x,k} = x_k + \left[\sigma_k\left(y_k^2 + 2\right) + \sigma_{k+1}\Delta_k\right]/(y_k - y_{k+1}) \end{cases} \tag{15}$$

where $\Delta_k = y_k^2 + 2y_k y_{k+1} - 2$.

The mentioned $N-1$ segment array curves are connected together to get the overall interpolation fitting array estimation curve.

For an assumption that the left scale of the y axis at the position of the sensor after the distortion is approximately unchanged under the built model, the coordinates of the y axis will actually be altered due to the distortion of the array. Thus, the estimated formation will be partially stretched. In other words, an error is identified in the estimation of the length of the curve between adjacent sensors, so the model error of this model can be defined as the difference between the curve length between the two adjacent sensors after distortion and the length of the undistorted array. The total error δ is all the accumulation of errors between adjacent sensors.

$$RMSE = \sqrt{\frac{1}{N}\sum_{i=1}^{n}\left((x_i - \widehat{x_i})^2 + (y_i - \widehat{y_i})^2 + (z_i - \widehat{z_i})^2\right)} \tag{16}$$

where $\widehat{x_i}, \widehat{y_i}, \widehat{z_i}$ represent the discrete point coordinates of the theoretical array fitting and x_i, y_i, z_i represent the discrete point coordinates of each segment of the array calculated based on the invariance of curve translation. Correspondingly, the root mean square errors of the $x-o-y$ and $y-o-z$ plane projection curves (*RMSEx and RMSEz*) are represented by Equation. (17).

$$\begin{cases} RMSEx = \sqrt{\frac{1}{N}\sum_{i=1}^{n}\left((x_i - \widehat{x_i})^2 + (y_i - \widehat{y_i})^2\right)} \\ RMSEz = \sqrt{\frac{1}{N}\sum_{i=1}^{n}\left((z_i - \widehat{z_i})^2 + (y_i - \widehat{y_i})^2\right)} \end{cases} \tag{17}$$

III. SIMULATION AND ERROR ANALYSIS

A. SYSTEM SIMULATION AND RESULTS DISCUSSION

The horizontal floating linear array is suitable for the detection of long-distance targets in the deep sea. Only when the scale of the array is larger and the array length is longer, the deformation of the array will be relatively large. At this time, the accurate estimation of the formation is very meaningful. The initial simulation conditions in this paper are: array length $L = 1000m$, the number of attitude depth sensors distributed on the array is $N = 50$, the angle between the anchor rope and the vertical direction is $\alpha = 30°$, the anchor rope length is $L_r = 200m$ and The distance of the sea surface to the bottom of the sea is $H = 500m$.

The steps of numerical solution are as follows:

- Convert the measurement data of the sensor into the coordinates of the point.
- Divide the y axis into n segments at equal intervals.
- Replace the curve with a straight line in each segment.
- The curve segment between two adjacent sensors is fitted with a quadratic curve to find the fitting coefficient.
- Define the estimated error as s, and set the upper limit of error as d.
- Determine the estimation error in the respective segment, and judge whether it exceeds the upper limit of the error. If it exceeds the upper limit, the interval is divided more finely; otherwise, continue to the next step.
- Fit all small segments of straight lines to yield the final formation curve.

B. MODEL ERROR ANALYSIS OF THE NUMBER OF SENSORS

The critical factor of the error of ITPF formation estimation model refers to the number of sensors. On the whole, the more the sensors, the more the information of the formation can be acquired. Under the identical distortion conditions, the formation curve estimated by adopting the same method exhibits higher accuracy. The following is an analysis of the effect of the number of sensors on the formation estimation error via simulation data.

It is assumed that the total length of the array is $L = 1000m$, the depth of the anchor bottom is $H = 500m$, the length of the anchor rope is $L_r = 250m$, and the angle between the anchor rope and the vertical direction $\alpha_1 = 30°$ at the initial moment, and the simulation data are adopted to analyze the model estimation error at $N = 5, 10, 15, \ldots, 100$.

By Equation.(16), the model error of different sensor numbers on the identical length array can be determined, as listed in TABLE 1.

TABLE 1. Model error of different number of sensors.

Number of sensors	Error/m	Number of sensors	Error/m
5	4.064208057	55	0.051599241
10	1.03621754	60	0.046914105
15	0.46854104	65	0.038733654
20	0.272291406	70	0.038152449
25	0.183883153	75	0.027475215
30	0.128203293	80	0.026990264
35	0.105005147	85	0.026764137
40	0.084209685	90	0.024383611
45	0.078673467	95	0.021740698
50	0.061493662	100	0.020651975

Taking the abscissa as the number of sensors and the ordinate as the model error, a graph of the relationship between the model error and the number of sensors is drawn in Fig. 5. As indicated from the figure, the model error decreases with the increase in the number of sensors, and the decreasing trend levels off, i.e., when the number of sensors reaches a certain threshold, continuing to increase the number of sensors cannot effectively increase the accuracy of the model.

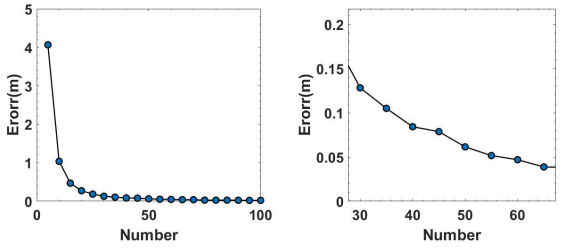

FIGURE 5. Model error graph for different sensor numbers.

It is reported that when the number of sensors reaches 10, the error of the model is 1.036m. Then, the error is close to the lowest point. For this reason, when only the factors affecting the number of sensors are considered, the optimal option in this model is that 10 sensors are distributed equidistantly.

C. MODEL ERROR ANALYSIS OF SENSOR MEASUREMENT ACCURACY

Since this study complies with the measurement data of the sensor to estimate the array curve, when the number and distribution of the sensor are fixed, the accuracy of the array estimation is primarily determined by the measurement accuracy of the sensor. In the practical measurement, the sensor regulates multiple measurements at one point. The results are inconsistent, but randomly distributed in a small area. Since this area is a random area centered on the original point, the fluctuation amplitude of the random area can be adopted to indicate the measurement accuracy of the sensor. At present, the pitch and roll angle measurement accuracy of common industrial attitude sensors on the market is nearly 0.5°, and the heading angle measurement accuracy is approximately 1°. The maximum depth measured in the example is 250m, and the measurement accuracy of the depth sensor is about 0.5m. To avoid the effect of mutual measurement accuracy, the measurement accuracy of other sensors can be set to a fixed value when selecting the accuracy range.

According to Fig. 6,Fig. 7 and Fig. 8, the relationship between the model error and the measurement accuracy of the sensor can be obtained. As revealed from the mentioned relationship diagram, with the gradual increase in the measurement error of the sensor, the model error increases, and the three relationship curves tend to be approximately linear, demonstrating that when the number and distribution position of the sensors remain unchanged, the model error increases with the measurement accuracy of the sensor linearly.

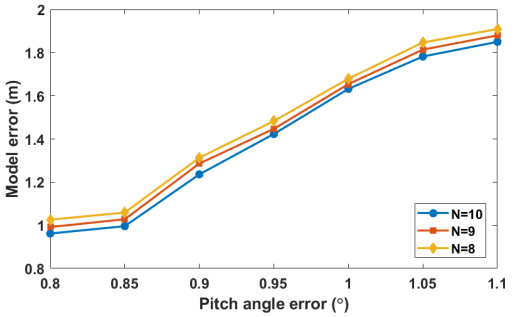

FIGURE 6. The curve of model error versus measurement error of deflection angle.

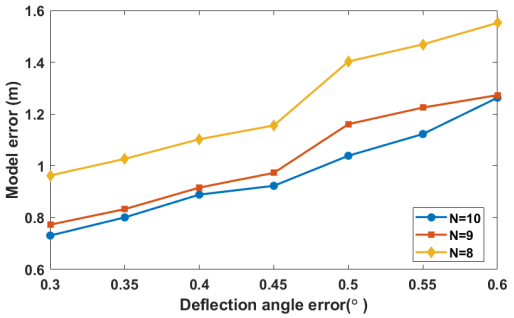

FIGURE 7. Variation curve of model error with pitch angle measurement error.

D. MODEL ERROR ANALYSIS OF SENSOR DISTRIBUTION POSITION

To analyze the effect of the sensor's distribution position on the model error, the present study designs three different sensor array methods, and analyzes the effect of the sensor's distribution position on the model error by calculating the model errors of the three methods.

1) SENSORS ARE EQUALLY SPACED

This method refers to the distribution method of the aforementioned sensors. M attitude and depth sensors are placed on a floating array of length L at equal distances (Fig. 2).

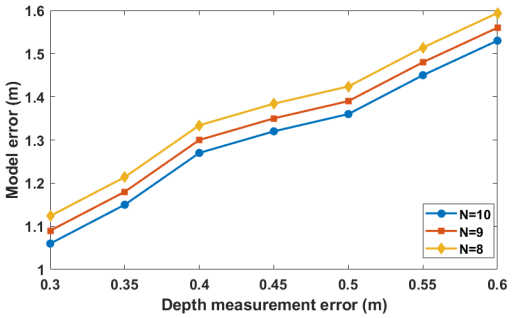

FIGURE 8. The curve of model error versus depth measurement error.

2) THE ENDS ARE DENSE AND THE MIDDLE IS SPARSE

As indicated from the conclusions in Section 2, the theoretical line type of the horizontal floating array is parabolic. Accordingly, to expedite calculation, the density of the middle density on both sides exhibits symmetrical distribution, and the degree of density from both ends to the middle can be determined with the adjacent sensors.

The distance between the two middle sensor units is taken as the length of each sensor unit. The YIS300 industrial-grade attitude sensor and the PTH601 depth sensor are taken as an example. The size of the former is $37.7 \times 24 \times 9.5mm$ and the size of the latter is $\phi 26 \times 110mm$. The length of the sensor unit consisting of two sensors reaches $120mm$, so the distance between the two adjacent sensors in the middle position is $0.12m$. N sensors exhibit their distribution on a floating array of length L, and the arithmetic sequence of the distribution expressed as Equation.(18):

$$\begin{cases} a_k = a_1 + (k-1)\,d \\ S_k = ka_1 + \dfrac{k\,(k-1)}{2}d \end{cases} \tag{18}$$

With the left half as an example (the right half is symmetrical for the central axis), the value of $a_{N/2}$ is known, and $S_{N/2} = L/2$, so the parameters a_1 and d of the arithmetic sequence can be determined.

3) SPARSE AT BOTH ENDS AND DENSE IN THE MIDDLE

Such layout method is also symmetrically distributed about the middle part of the array. The difference from the dense middle and sparse sides lies in the smaller distance between the middle and the two ends. The arithmetic sequence is still complied with when the distance between adjacent sensors are being calculated.

According to the sensor measurement data in the calculation example and the simulation method of the model, the model errors of the three different layout modes are determined (TABLE 2).

As revealed from the results of the presented table, the model error is the minimum when the two ends are dense and the middle is sparse. This is because under the identical distortion conditions, the deformation at the two ends of the floating array is larger than the deformation at the middle position, and the two ends exhibit more significant distribution. When there are more sensors, the more detailed the array distortion information acquired, the smaller the fitting error will be when interpolation fitting is being performed.

TABLE 2. Model errors of different sensor placement methods.

Array layout	Isometric placement	Dense in the middle and sparse at both ends	Sparse at both ends and dense in the middle
Model error (m)	0.231	0.913	0.197
Distance between sensors(m)	10	1.2∼19.2	1.2∼19.2

4) MINIMUM ARRAY DISTANCE AT DIFFERENT POSITIONS OF THE ARRAY

The previous section is to study the effect of the sensor array method on the model error through qualitative analysis, and further we define the minimum array distance at different positions on the array as the quantitative standard for array sensor.

When the distance between adjacent sensors on the array is excessively small, as impacted by the measurement error of the attitude angle of the sensor, the curve slope changes cannot be distinguished at the two sensor positions.

It is assumed that the measurement errors of pitch angle and yaw angle are $\delta\theta$ and $\delta\varphi$ respectively, the minimum array distance that meets the measurement accuracy of the sensor is D_k. Since the measurement error is overall small ($\sim 1°$), there are approximate formulas $\delta\theta \approx \tan(\delta\theta)$ and $\delta\varphi \approx \tan(\delta\varphi)$, to enable the sensor to sense the change of the attitude angle, it needs to satisfy Equation.(19).

$$\begin{cases} \delta\theta \le \Delta\theta_k \\ \delta\varphi \le \Delta\varphi_k \end{cases} \tag{19}$$

where $\Delta\theta_k$ and $\Delta\varphi_k$ denote the pitch and yaw angle changes at the two ends of the k-th segment of the sub-curve.

$$\begin{cases} \Delta\theta_k = \theta_{k+1} - \theta_k \\ \Delta\varphi_k = \varphi_{k+1} - \varphi_k \end{cases} \tag{20}$$

According to the two-angle difference formula of the tangent, the angle variation range of the Equation.(20) is calculated together with the Equation.(5).

$$\begin{cases} \delta\theta \le \dfrac{\kappa_{k+1} - \kappa_k}{1 + \kappa_{k+1} \cdot \kappa_k} \\ \delta\varphi \le \dfrac{\sigma_{k+1} - \sigma_k}{1 + \sigma_{k+1} \cdot \sigma_k} \end{cases} \tag{21}$$

With a given angle accuracy, the corresponding y_k and y_{k+1} can be calculated by Equation.(20), and the coordinate information can be obtained using the parameter matrix calculated by the model, and then the minimum array distance can be obtained as shown in Equation.(21).

$$D_k = \sqrt{(x_{k+1} - x_k)^2 + (y_{k+1} - y_k)^2 + (z_{k+1} - z_k)^2} \tag{22}$$

Take the pitch angle measurement accuracy as 0.5° and the yaw angle measurement accuracy as 1°. According to the data

TABLE 3. Minimum array distance at different positions.

k	$D_k\ (m)$	k	$D_k\ (m)$
1	6.92	60	48.45
10	15.6	70	30.17
20	20.14	80	20.9
30	25.65	90	10.32
40	35.78	99	5.06
50	45.57		

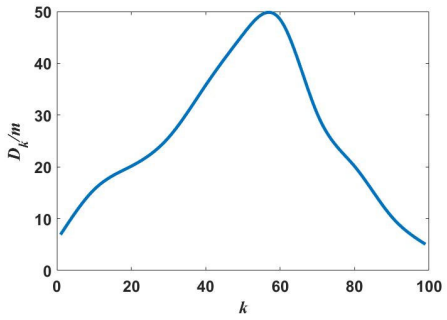

FIGURE 9. The minimum array distance of different positions on the array.

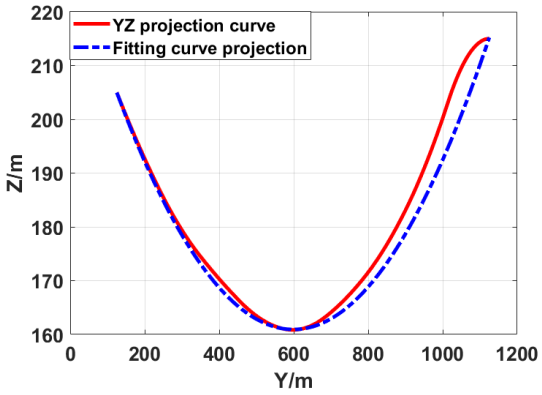

FIGURE 10. The projection curve of the formation curve on the y-O-z plane.

in the calculation example, calculate the minimum distance of the array at different positions as shown in TABLE 3.

Fig. 9 is a graph showing the relationship between k and the minimum array distance of the sensor. As indicated from the figure, the minimum distribution distance of the sensor decreases with the increase in the array distortion. The array distortion is the minimum at the middle of the array, and the sensor is capable of identifying the maximal distribution distance.

E. ANALYSIS OF SIMULATION RESULTS OF ESTIMATING FORMATION CURVE

By the mentioned model accuracy analysis, the measurement accuracy of the attitude sensor's deflection angle is taken as 1°, the measurement accuracy of the pitch angle is 0.5°, and the measurement accuracy of the depth sensor is $0.5m$, and the simulation is performed to estimate the formation

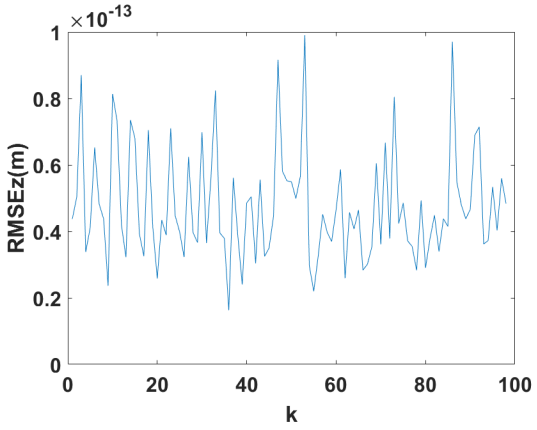

FIGURE 11. The root mean square error RMSEz on the y-o-z plane projection curve.

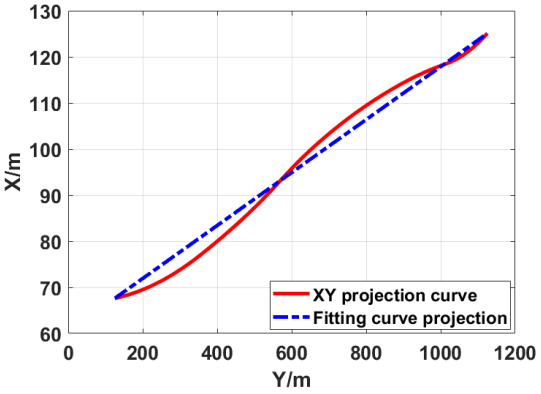

FIGURE 12. The projection curve of the formation curve on the x-O-y plane.

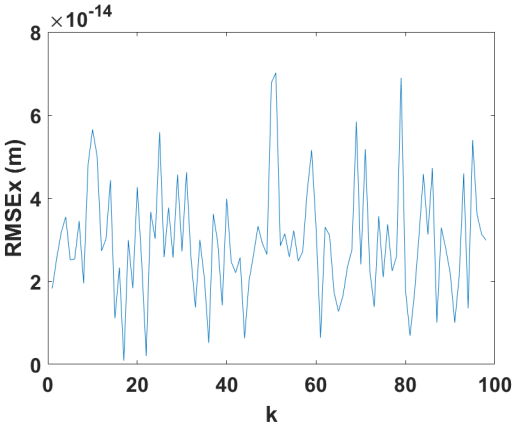

FIGURE 13. The root mean square error RMSEz on the x-o-y plane projection curve.

curve. It is reported that under the array length of $L = 1000m$, the array mode of close at both ends and sparse in the middle is selected, and the distance between two adjacent sensors is not less than the minimum array distance.

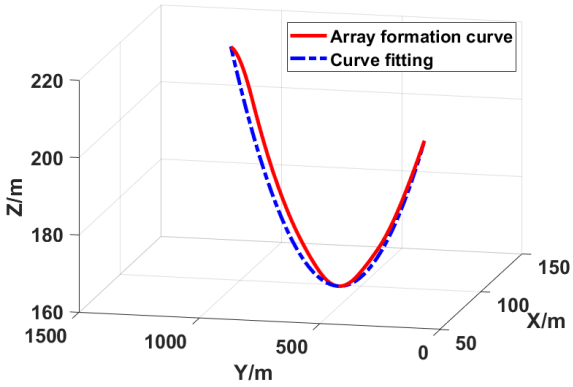

FIGURE 14. Three-dimensional curve of array and fitting formation curve.

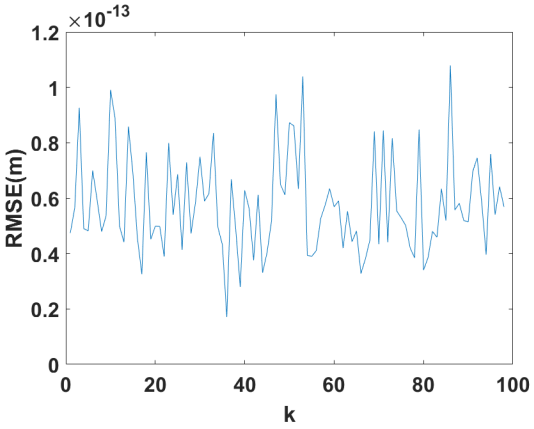

FIGURE 15. The root mean square error RMSE between the model simulation actual curve and the theoretical curve.

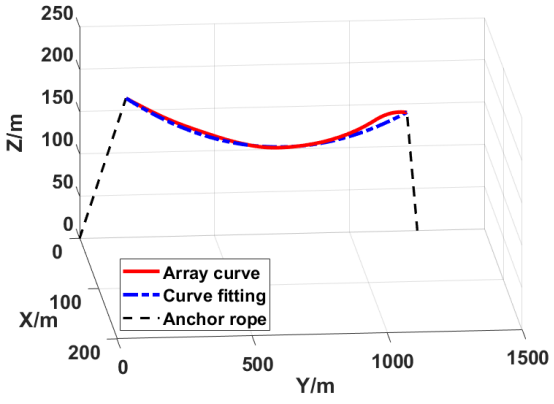

FIGURE 16. The actual array layout after the formation correction.

By solving the corresponding parameter matrix, and all the sub-curve segments are connected to plot the simulation curve of the formation. Fig. 10and Fig. 12 illustrate the projections of the formation estimation curve in two planes, both of which are parabolic, complying with the theoretical line derived from the theoretical derivation. Fig. 16 presents the suspension diagram of the estimated formation curve of the horizontal suspension array. The model error reaches 1.036m, the error is relatively small relative to the array length, and the accuracy is high.

IV. CONCLUSION

This paper designs a real-time estimation of the formation of a horizontally suspended linear array based on depth and attitude sensors. Through the sensor output angle and pressure information at each moment, the accuracy of the formation state function can be solved by using the translation invariance of the curve. Determine the equations and concatenate them to get the estimated curve. Through comparison with the theoretical formation curve and error analysis, it is found that the estimated formation is basically consistent with the theoretical formation and the error is small. Through simulation, the error of this method changes with the number of sensors and measurement accuracy, and the correctness of the method is initially verified. The shortest sensor array distance at different sensor positions is further quantitatively analyzed. This analysis method can It provides a theoretical basis for the defense of the actual array sensor. The simulation parameters are optimized through error analysis. The optimized result has smaller errors than before optimization, and fewer sensors are used. In addition, this method is also applicable to the formation estimation of other array forms except the floating array, and has good universality.

ACKNOWLEDGMENT

(Zonglun Che and Jun Wang contributed equally to this work.)

REFERENCES

[1] O. Fangming, "Research on the formation method of small-scale side array," *Acoust. Electron. Eng.*, vol. 1, no. 121, pp. 40–43, 2016.
[2] Z. Dong, "The mathematical model of target motion analysis of side array sonar," *Electro-Opt. Control*, vol. 2, no. 14, pp. 16–19, 2007.
[3] C. Chi, V. Pallayil, and M. Chitre, "Design of an adaptive noise canceller for improving performance of an autonomous underwater vehicle-towed linear array," *Ocean Eng.*, vol. 202, Apr. 2020, Art. no. 106886.
[4] Y. Wang, Z. Gong, and R. Zhang, "Phase correction in extended towed array method," *J. Acoust. Soc. Amer.*, vol. 141, no. 5, p. 3916, 2017.
[5] C. Peng and X. Zhang, "A dynamic depth estimation method for towed optical fiber hydrophone array," *J. Acoust. Soc. Amer.*, vol. 143, no. 5, pp. EL399–EL404, May 2018.
[6] C. Li, J. Jiang, F. Duan, X. Wang, L. Ma, L. Bu, and Z. Sun, "Towed array shape estimation based on single or double near-field calibrating sources," *Circuits, Syst., Signal Process.*, vol. 38, no. 1, pp. 153–172, Jan. 2019.
[7] D. V. A. N. R. Kumar, S. K. Rao, and K. P. Raju, "Estimate-merge-technique-based algorithms to track an underwater moving target using towed array bearing-only measurements," *Sadhana*, vol. 42, no. 9, pp. 1617–1628, Sep. 2017.
[8] S. Niu, X. liang, M. Ni, and Y. Hu, "Research on array estimation method of shore-based hydrophone array," *Acoust. Electron. Eng.*, vol. 2, no. 7, pp. 7–9, 2006.
[9] Y. Chen, F. Gao, Q. Yang, and Z. Ma, "Sound source localization performance of shallow sea short vertical array and rare vertical array," *Acta Acoustica*, vol. 6, no. 11, pp. 912–921, 1996.
[10] J. Wang, J. Zhu, W. Chen, P. Xu, Y. Zou, Y. Wu, and Z. Hu, "Array shape estimation of a horizontal suspension hydrophone line array," *IEEE Sensors J.*, vol. 20, no. 3, pp. 1550–1557, Feb. 2020.
[11] W. Shulin and L. Shuqiu, "Minimum length of damping section for towed array based on revised paidoussis equation," *Electron. Lett.*, vol. 53, no. 14, pp. 958–960, Jul. 2017.

[12] J. J. Smith, Y. H. Leung, and A. Cantoni, "The partitioned eigenvector method for towed array shape estimation," *IEEE Trans. Signal Process.*, vol. 44, no. 9, pp. 2273–2283, Sep. 1996.
[13] N. C. Wyeth, "Methods of array element localization for a towed underwater acoustic array," *IEEE J. Ocean. Eng.*, vol. 19, no. 1, pp. 128–133, Jan. 1994.
[14] H. Bucker, "Beamforming a towed line array of unknown shape," *J. Acoust. Soc. Amer.*, vol. 63, no. S1, p. S48, May 1978.
[15] B. G. Ferguson, D. A. Gray, and J. L. Riley, "Comparison of sharpness and eigenvector methods for towed array shape estimation," *J. Acoust. Soc. Amer.*, vol. 91, no. 3, pp. 1565–1570, Mar. 1992, doi: 10.1121/1.402437.
[16] Y. Rockah and P. Schultheiss, "Array shape calibration using sources in unknown locations—Part I: Far-field sources," *IEEE Trans. Acoust., Speech, Signal Process.*, vol. 35, no. 3, pp. 286–299, Mar. 1987.
[17] J. J. Smith, Y. H. Leung, and A. Cantoni, "The Cramér–Rao lower bound for towed array shape estimation with a single source," *IEEE Trans. Signal Process.*, vol. 44, no. 4, pp. 1033–1036, Apr. 1996.
[18] D. E. Wahl, "Towed array shape estimation using frequency-wavenumber data," *IEEE J. Ocean. Eng.*, vol. 18, no. 4, pp. 582–590, Oct. 1993.
[19] J. J. Smith, Y. H. Leung, and A. Cantoni, "The partitioned eigenvector method for towed array shape estimation," in *Proc. Int. Conf. Acoust., Speech, Signal Process.*, vol. 5, 1995, pp. 3103–3106.
[20] P. Tichavsky and K. T. Wong, "Quasi-fluid-mechanics-based quasi-Bayesian Cramér–Rao bounds for deformed towed-array direction finding," *IEEE Trans. Signal Process.*, vol. 52, no. 1, pp. 36–47, Jan. 2004.
[21] N. V. Nikitakos, A. K. Leros, and S. K. Katsikas, "Towed array shape estimation using multimodel partitioning filters," *IEEE J. Ocean. Eng.*, vol. 23, no. 4, pp. 380–384, Oct. 1998.
[22] G. H. Kim, S. J. Choi, C. S. Ryu, Y. W. Ryu, and K. K. Lee, "Towed array shape estimation based on Kalman filter compensating the sensor bias," *J. Korea Inst. Mil. Sci. Technol.*, vol. 19, no. 2, pp. 155–162, Apr. 2016.
[23] J. L. Riley and D. A. Gray, "Towed array shape estimation using Kalman filters-experimental investigations," *IEEE J. Ocean. Eng.*, vol. 18, no. 4, pp. 572–581, Oct. 1993.
[24] H.-Y. Park, D.-H. Youn, C. Lee, H. W. Kang, K.-M. Kim, and K.-C. Dho, "Evaluation of the calibration method using iterative spline interpolation for array shape estimation," in *Proc. MTS/IEEE Techno-Ocean*, vol. 2, Nov. 2004, pp. 593–597.
[25] C. M. Ablow and S. Schechter, "Numerical simulation of undersea cable dynamics," *Ocean Eng.*, vol. 10, no. 6, pp. 443–457, Jan. 1983. [Online]. Available: https://www.osti.gov/biblio/6457639
[26] F. Lu, E. Milios, S. Stergiopoulos, and A. Dhanantwari, "New towed-array shape-estimation scheme for real-time sonar systems," *IEEE J. Ocean. Eng.*, vol. 28, no. 3, pp. 552–563, Jul. 2003.
[27] B. E. Howard and J. M. Syck, "Calculation of the shape of a towed underwater acoustic array," *IEEE J. Ocean. Eng.*, vol. 17, no. 2, pp. 193–203, Apr. 1992.
[28] M. P. Paidoussis, "Dynamics of flexible slender cylinders in axial flow part 1. Theory," *J. Fluid Mech.*, vol. 26, no. 4, pp. 717–736, 1966.
[29] B.-K. Yang, K.-Q. Zhu, Y.-J. Zhu, and D.-W. Qin, "Dynamic response of towed line array," *J. Hydrodyn., B*, vol. 25, no. 4, pp. 616–619, Aug. 2013.

ZONGLUN CHE received the B.S. degree in optical engineering from the College of Optoelectronic Science and Engineering, National University of Defense Technology (NUDT), in 2020, where he is currently pursuing the M.S. degree with the Laboratory of Deep Ocean Science and Technology.

His current research interests include array shape estimation and underwater signal processing.

JUN WANG received the B.S. degree in optical information science and technology and the Ph.D. degree in optical engineering from the College of Optoelectronic Science and Engineering, National University of Defense technology (NUDT), in 2010 and 2016, respectively.

During his Ph.D. degree, he studied as a joint Ph.D. candidate (for one year) at the University of New South Wales, Australia, in 2013. Since 2016, he has been a Lecturer with the Academy of Ocean Science and Engineering, NUDT, where he is currently an Assistant Professor with the College of Meteorology and Oceanography. His current research interests include FBG sensors, fiber optic sensing, photo-electrical signal processing, and fiber optic hydrophone technologies.

JING ZHU received the B.S. degree in optical information science and technology, and the M.E. and Ph.D. degrees in optical engineering from the College of Optoelectronic Science and Engineering, NUDT, Changsha, China, in 2010, 2012, and 2017, respectively.

She is currently a Lecturer with the College of Meteorology and Oceanography, NUDT. Her current research interests include fiber optic sensing and inertia navigation.

BINGBING ZHANG received the B.S. degree in electronic engineering, the M.S. degree in electronic science and technology, and the Ph.D. degree in information and communication engineering from the National University of Defense Technology (NUDT), Changsha, China, in 2011, 2013, and 2018, respectively.

From June 2016 to June 2017, he visited the Department of Automation, Shanghai Jiao Tong University, China. He is currently an Assistant Research Fellow with the College of Meteorology and Oceanography, NUDT. His main research interests include underwater localization, navigation, and target tracking.

YANG ZHANG received the B.S. degree in optical engineering from the College of Optoelectronic Science and Engineering, National University of Defense Technology (NUDT), in 2013, where he is currently pursuing the M.S. degree with the Laboratory of Deep Ocean Science and Technology.

His current research interests include array shape estimation and underwater signal processing.

YANQUN WU received the B.S. degree in optoelectronic engineering and the Ph.D. degree in optical engineering from the National University of Defense Technology, in 2004 and 2011, respectively.

Since 2011, she has been a Lecturer with the Research Laboratory of Optical Information, College of Optoelectronic Science and Engineering, NUDT, where she is currently a Lecturer with the College of Meteorology and Oceanography. Her research interests include optical fiber sensing, optical fiber laser, optical fiber gyroscope, and optical communication.